CM² MAGAZINE

第 32 期

南方科技大学海洋磁学中心主编

创刊词

海洋是生命的摇篮，是文明的纽带。地球上最早的生命诞生于海洋，海洋里的生命最终进化成了人类，人类的文化融合又通过海洋得以实现。人因海而兴。

人类对海洋的探索从未停止。从远古时代美丽的神话传说，到麦哲伦的全球航行，再到现代对大洋的科学钻探计划，海洋逐渐从人类敬畏崇拜幻想的精神寄托演变成可以开发利用与科学研究的客观存在。其中，上个世纪与太空探索同步发展的大洋科学钻探计划将人类对海洋的认知推向了崭新的纬度：深海（deep sea）与深时（deep time）。大洋钻探计划让人类知道，奔流不息的大海之下，埋藏的却是亿万年的地球历史。它们记录了地球板块的运动，从而使板块构造学说得到证实；它们记录了地球环境的演变，从而让古海洋学方兴未艾。

在探索海洋的悠久历史中，从大航海时代的导航，到大洋钻探计划中不可或缺的磁性地层学，磁学发挥了不可替代的作用。这不是偶然，因为从微观到宏观，磁性是最基本的物理属性之一，可以说，万物皆有磁性。基于课题组的学科背景和对海洋的理解，我们对海洋的探索以磁学为主要手段，海洋磁学中心因此而生。

海洋磁学中心，简称 CM^2，一为其全名“Centre for Marine Magnetism”的缩写，另者恰与爱因斯坦著名的质能方程 $E = MC^2$ 对称，借以表达我们对科学巨匠的敬仰和对科学的不懈追求。

然而科学从来不是单打独斗的产物。我们以磁学为研究海洋的主攻利器，但绝不仅限于磁学。凡与磁学相关的领域均是我们关注的重点。为了跟踪反映国内外地球科学特别是与磁学有关的地球科学领域的最新研究进展，海洋磁学中心特地主办 CM^2 Magazine，以期与各位地球科学工作者相互交流学习、合作共进！

“海洋孕育了生命，联通了世界，促进了发展”。 21 世纪是海洋科学的时代，由陆向海，让我们携手迈进中国海洋科学的黄金时代

目 录

第 22 章　沉积剩磁 DRM

SD 颗粒的 TRM 基于尼尔理论，在不发生热转化的情况，我们只需要简单地加热降温等手段就可以在实验室合理地模拟 TRM（pTRM）过程。能够记录 TRM 的自然介质主要为火山岩，尤其是玄武岩这种喷发岩，喷发快冷却快，于是形成的磁铁矿颗粒一般都很小，能够记录稳定的剩磁。对于那些侵入岩，比如花岗岩，其冷却时间非常长，所以可以结晶出大颗粒的磁铁矿。结晶时间长还对应着另外一个弊端，就是一块样品记录的是很长一段时间内地磁场的综合响应。所以，目前基本不会用花岗岩来研究古地磁场的变化。

另外考古中用的瓷片、陶片、砖头瓦罐等等都要经过煅烧过程，于是也能记录 TRM，是考古磁学研究的上乘材料。

前面提及，洋壳是玄武岩喷发后形成的，符合 TRM 原理。所以，可以把海底洋壳钻取上来进行研究，不过这可不是一件容易的事情。如果碰到 IODP 航次要钻取洋壳样品，就要赶紧申请参加。处于保护机制，谁上船工作，谁就优先研究这些岩石，等过了保密期以后，其他人才能申请。

这些 TRM 信息较为准确，但是时间上不连续。我们不能要求一座火山定时定点地喷发。考古材料只能用来研究过去几千年的历史，而地质历史已经好几十亿年，根本就不匹配。洋壳能够用来研究过去最多一亿年以来的故事，但是洋壳样品非常难以获得。

我们把目光转移到另外一种非常常见的介质，沉积物。湖底或者河底的淤泥，就是沉积物。用手一捞，松松散散的一团泥巴，这个也能记录古地磁信息？

在环境比较稳定的情况，沉积物会越积越厚，在重力压实作用下，水分会慢慢析出，最后经过成岩作用，慢慢变成了沉积岩。

在沉积物中，常常会含有磁性矿物。这些磁性矿物一般都拥有一个初始磁化强度，可能是 TRM，也可能是 CRM。在地磁场的作用下，这些磁颗粒的 M 会沿地磁场方向发生偏转。最后在沉积压实过程中，磁性颗粒慢慢被基质锁定（lock-in），从而记录了地磁场的信息，当然也包括地磁场的方向和强度，我们把该剩磁

成为沉积剩磁或碎屑剩磁（depositional/detrital remanent magnetization, DRM）。

我们会发现，在水-沉积物交界面以下几公分到十几公分的深度，沉积物中含水量太高，以至于磁性颗粒可以自由地发生偏转，不能有效地记录地磁场信息。只有在这个深度之下，磁性颗粒才能在压实作用下固定下来。我们称这个深度为 DRM 锁定深度（Lock-in depth）。

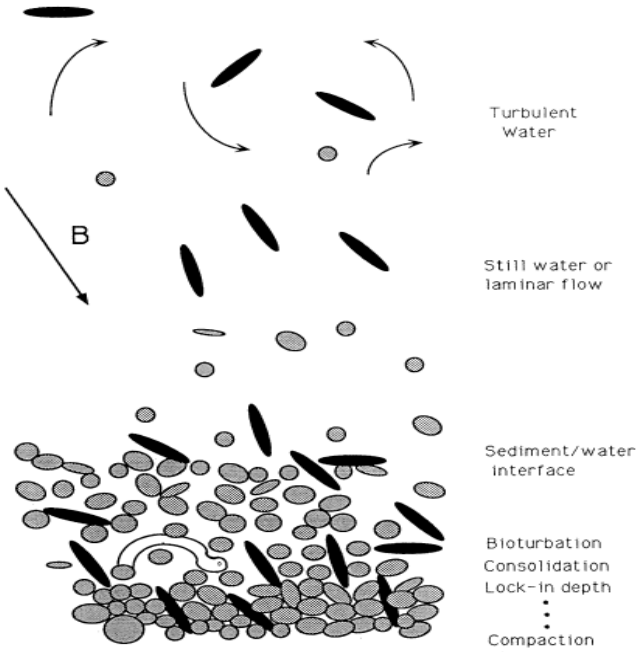

图 1 磁性矿物在沉积过程，记录地磁场信息的过程。

除了锁定深度，在其之上我们还要考虑一个表层混合（Surficial mixing layer, SML）深度。海底并不平静，那里还生活着不少生物，比如虾、螃蟹、鱼等等。它们会搅动海底的淤泥，使得 SML 这一层里的磁性矿物不断地沉积再扰动，然后再沉积。如何判断这一层有多厚呢？工业社会以来，人类制造了很多自然界没有的东西，比如微塑料和工业相关的各种污染物等。这些物质由于混合作用，会在表层分布。一般情况下，SML 的厚度为几个厘米。

在 SML+lock-in 深度之下，磁性颗粒会逐渐被固定，从而记录了和地磁场相关的沉积剩磁 DRM。实验表明，DRM 和地磁场呈现正相关关系。

但是，我们不能把 DRM 理解成 TRM。后者是在解阻情况，M 向 H_0 方向排列，当然肯定不能齐刷刷地排列过去，那就会得到 M_s，这显然不是事实。在获

得 DRM 过程中，磁性颗粒的排列效率更低。通过计算模拟显示，其实，只要每个颗粒朝向 H_0 偏转一点点，对于一个样品来说，其 DRM 就已经和 H_0 正相关了。

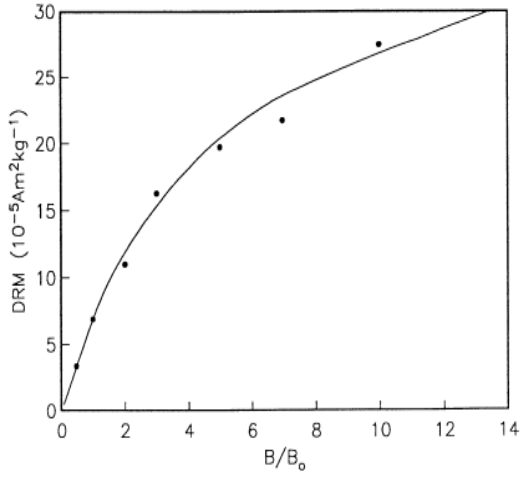

图 2 DRM 与外场之间的关系。当外场较小时，二者线性相关。

在沉积物沉积过程中，磁性颗粒很难独自行动，而是经常和其它颗粒聚集在一起（flocculation），形成更大的颗粒。这就使得 DRM 成为一种非常复杂的天然剩磁。DRM 的形成过程会和非磁性的基质以及水溶液的离子浓度密切相关，离子浓度的变化决定着颗粒之间的汇聚状态。

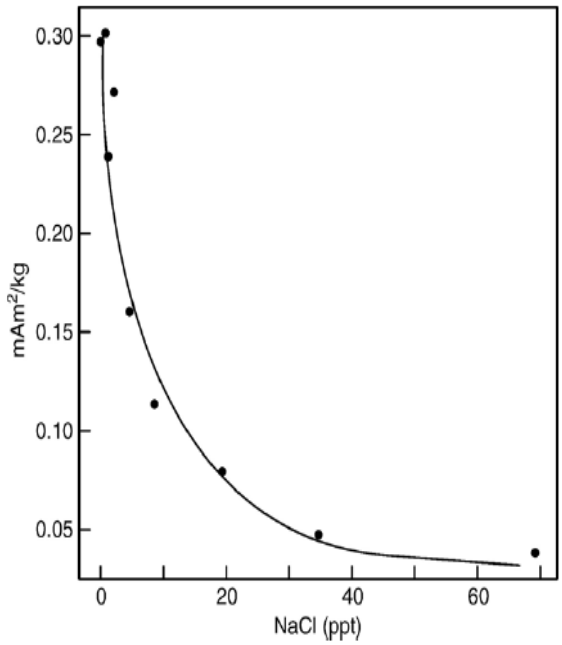

图 3　DRM 与 Nacl 浓度的关系图。

在实验室中，我们可以模拟这些因素的影响。比如我们不用纯净水，而是用含有一定浓度的 NaCl 进行沉积实验。结果表明，随着 NaCl 浓度的增加，DRM 的强度迅速降低。当 NaCl 的含量超过 30 ppt 时，趋于稳定。

离子浓度的变化直接影响颗粒表面的电荷分布，进而影响颗粒度的聚集过程。可见离子浓度变化的影响甚至会超过外场的作用。

目前对海洋沉积物的 DRM 研究，成果颇丰，而对湖相和边缘海沉积物的研究则滞后很多。大部分情况下，后者很难得到较为合理的 DRM 结果。虽然没有深入研究，我猜想应该有如下两个主要因素：

第一个就是离子浓度的变化。无论是湖还是边缘海，水深很浅。湖水蒸发会造成离子浓度的增加。边缘海更是淡水和海水交界的地方，水中离子浓度也会变化较大。

第二个因素就是，这些沉积环境里，物质颗粒变化很大，不均一性太大，不适合 DRM 研究。

对于磁性颗粒而言，比如磁铁矿，多大的粒径适合记录 DRM？

SP 颗粒肯定不行，因为它任何剩磁都不记录。

SD 颗粒能记录稳定的 TRM，它们能记录稳定的 DRM 吗？虽然单个 SD 颗粒能够记录一个稳定磁化强度，但是 DRM 是这些颗粒的磁化强度再次发生旋转而获得的。SD 颗粒太小，在沉积物中容易发生物理转动，因而并不是一种可靠的载体。

MD 颗粒也不是最佳的载体，因为它的剩磁既不稳定，本身由于颗粒太大，在外场中的偏转效率不高，而且也容易受到扰动的影响。

那最后只剩下 PSD 颗粒了。实验证实，PSD 颗粒才是记录 DRM 的主力军。在自然界中，大部分情况都是以 PSD 颗粒占主导。

文献导读

1. 甲烷渗漏型冷泉碳酸盐岩中微量元素的潜力、局限性和发展前景

D. Smrzka, D. Feng, T. Himmler et al., ***Trace elements in methane-seep carbonates: Potentials, limitations, and perspectives*** *[J]. Earth-Science Reviews, 208, 10263.*

https://doi.org/10.1016/j.earscirev.2020.103263.

摘要：海洋自生碳酸盐岩形成与浅水微生物岩、泥丘及甲烷渗漏型矿产，其中含有相当数量的微量元素，可以提供宝贵的古环境信息。由于许多微量元素对氧化还原反应都非常敏感，并参与其生物循环过程，因此部分碳酸盐岩的元素模式可以很好的记录地质历史时期的代谢过程。微量元素分布在生物碳酸盐中不仅解释古海洋中氧化还原信息，还可以揭示地球中水圈和大气圈的化学演化过程。微量元素模式可以用来区分海洋和淡水的来源，估计水深，并有助于查明微生物随时间变化的代谢过程。其中有个重要的问题是关于海洋碳酸盐岩可以用来指示早期和晚期成岩蚀变程度的古环境指标，这种蚀变的过程可有改变甚至重置微量元素的原始含量和分布。因此早期和后期成岩蚀变的程度可以通过对比有机和无机地球化学指标的元素含量进行评价。自生性甲烷渗漏型碳酸盐岩形成海底沉积物中，是甲烷和其他碳氢化合物的微生物氧化作用的产物。渗漏型碳酸盐可以作为很好的地质载体，其微量元素可以提供沉积氧化还原过程的信息，以及渗漏强度和流体组成等信息。微量元素在流体渗漏和化学合成形成的动态过程中发挥无可替代的作用，可以帮助重建显生宙时期以化学合成为基础的生命演化过程。

ABSTRACT: Marine authigenic carbonates form shallow-water microbialites, mud mounds, and hydrocarbon-seep deposits and contain appreciable amounts of trace elements that yield information on paleoenvironments. Element patterns of some of these carbonates archive metabolic processes through geologic time since many trace elements are redox-sensitive and participate in biological cycling. Trace element distributions in microbial carbonates not only yield information on the redox state of ancient oceans, but also on the chemical evolution of Earth's hydrosphere and atmosphere. Trace element patterns can be used to distinguish marine from freshwater sources, to estimate water depth, and can help identify microbial metabolisms through time. A major issue concerning the use

of marine carbonates as a paleoenvironmental archive is assessing the degree of early and late diagenetic alteration, which can modify or even reset the original content and distribution of trace elements. The degree and effect of early and late diagenetic alteration can be evaluated by comparing element contents to organic and other inorganic geochemical proxies. Authigenic hydrocarbon-seep carbonates forming in seafloor sediments are the product of microbial oxidation of methane and other hydrocarbon compounds. Seep carbonates are excellent archives, whose trace element contents yield information on sedimentary redox processes, as well as information on seepage intensity and fluid composition. Trace elements serve as proxies in these highly dynamic environments shaped by fluid seepage and chemosynthesis, and can help to reconstruct the evolution of chemosynthesis-based life at seeps through the Phanerozoic.

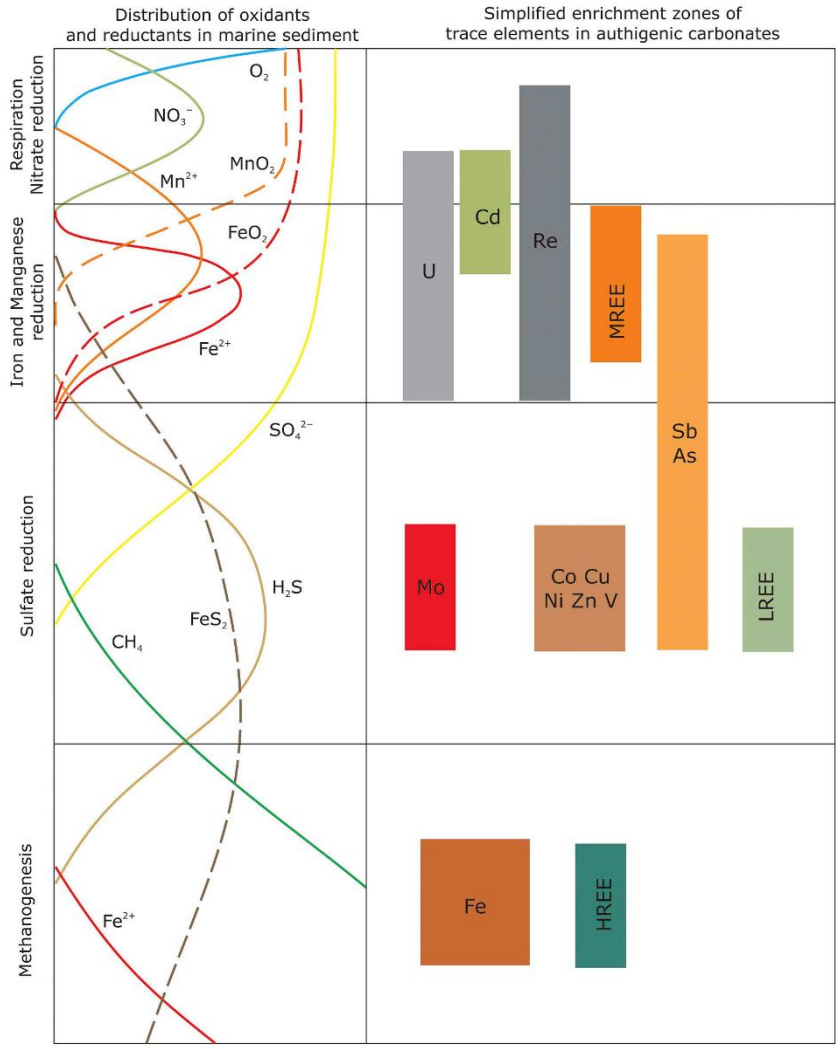

Figure 1. Left panel: Distribution of oxidants and reductants in seafloor sediments (after Froelich et al., 1979). Right panel: Distribution of trace and rare earth element enrichments in marine sediments (after Smrzka et al., 2019a and references therein). No scale implied. See text for details.

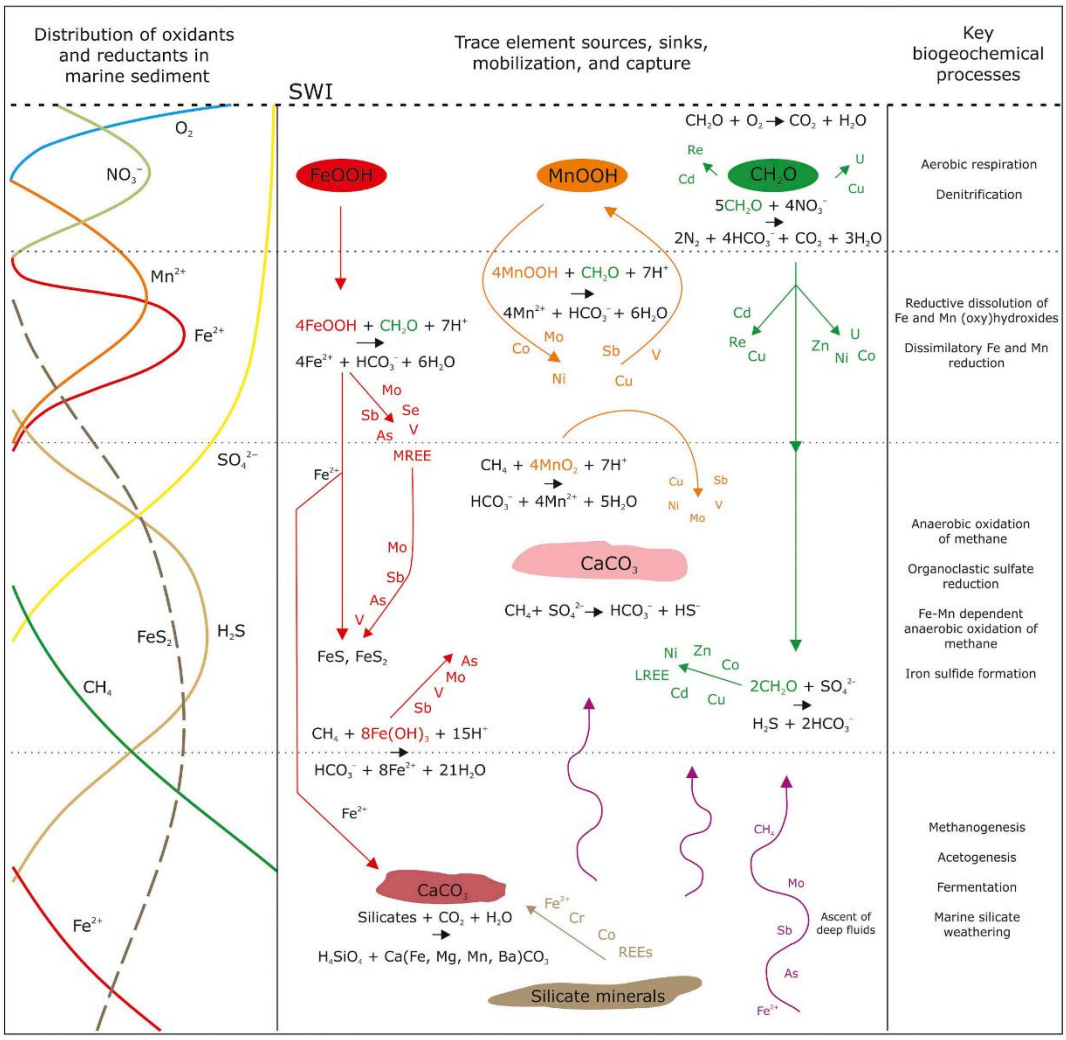

Figure 2. Left panel: Distribution of oxidants and reductants in marine sedimentary pore water. Middle panel: Schematic illustration of sources and sinks of trace elements in marine sedimentary pore water. Right panel: Key biogeochemical processes associated with the respective redox zones in marine sediments. SWI = sediment-water interface. No scale implied. See text for details.

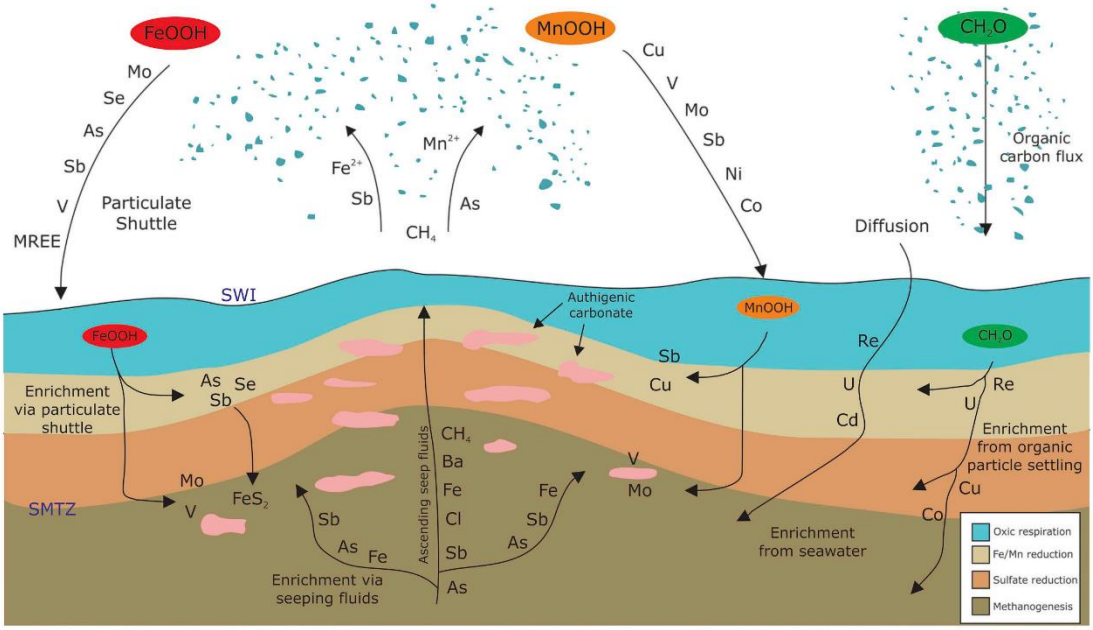

Figure 3. Schematic illustration of trace element enrichment processes at seeps. Ascending reduced fluids transport trace elements from deeper sediment layers towards the sulfate reduction zone where carbonate formation occurs. Seepage fluids are expelled to bottom waters where dissolved reduced iron and manganese are oxidized to precipitate iron and manganese (oxy)hydroxides particulates. These particulate phases selectively adsorb dissolved trace elements from seawater, and transport them back to seafloor sediments via the particulate shuttle. Diffusion from seawater and organic carbon flux from the photic zone selectively recharge sedimentary pore waters with trace elements. SWI = sediment-water interface; SMTZ = sulfate-methane transition zone. No scale implied. See text for details

2. 现今以及新生代腕足类的锂同位素组成

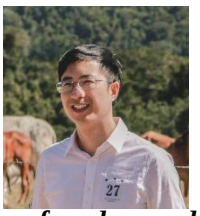

翻译人：蒋晓东 jiangxd@sustech.edu.cn

Washington K E, West A J, Kalderon-Asael B, et al. ***Lithium isotope composition of modern and fossilized Cenozoic brachiopods*** *[J].* ***Geology****, 2020, 48. https:// doi.org/10.1130/G47558.1*

摘要：以 δ^7Li_{sw} (‰)为代表的海水锂同位素记录了地史时期全球气候演化与碳循环信息。基于有孔虫的锂同位素分析表明在过去 60 百万年间 δ^7Li_{sw} 增高约 9‰，这被认为反应了这期间硅酸盐风化状态的变化，该风化有助于全球变冷。然而培养实验表明有孔虫的活性效应可能引起 δ^7Li 分馏变化，因而影响过去的记录。意味着需要借助其他的介质来判定有孔虫 δ^7Li 变化是否反映了新生代海水 δ^7Li 的长期变化。这种介质也需要具备长时间尺度的海水 δ^7Li 记录。本研究分析了 34 个现今腕足类的 δ^7Li 组成，发现具有相对窄的变化区间（+24.2 ‰—+28.8‰ （平均值 +26.8‰; 1σ = 0.5‰）），该值与海水沉积的无机方解石具有类似的变化区间。这些结果表明腕足类是研究海水 δ^7Li 的良好介质。本研究分析了 60 百万年到 700 千年期间腕足类化石的 δ^7Li 组成，发现腕足类的 δ^7Li 记录与有孔虫具有相似的变化特征。这些结果第一次证实新生代海水 δ^7Li 约 9‰的增长，该方法有潜力在有孔虫演化前而得到长时间尺度可靠的海水 δ^7Li 记录。

ABSTRACT： Seawater lithium stable isotope ratios, represented by δ^7Li_{sw} (‰), hold key information about the evolution of global climate and the carbon cycle over geologic time. Reconstructions based on foraminifera suggest an ~9‰ increase in δ^7Li_{sw} over the past 60 m.y., interpreted as reflecting changes in the silicate weathering regime that may have contributed to global cooling over this time. However, culture experiments suggest that vital effects in foraminifers might cause varied δ^7Li fractionation that could have affected past records. Thus, other archives are needed to determine whether the observed rise in foraminifer δ^7Li values over the Cenozoic indeed reflects secular changes in δ^7Li_{sw}. Such archives would also open possibilities for robust determination of δ^7Li_{sw} deeper in geologic time. We analyzed δ^7Li compositions in modern brachiopods (n = 34) and found a relatively narrow range of +24.2 ‰ to +28.8‰ (mean = +26.8‰; 1σ = 0.5‰), similar to the range reported for inorganic calcite precipitated from seawater. These results confirm that brachiopods are good candidates for providing a representative record of δ^7Li_{sw}. We present

data from fossil specimens dating from 65 Ma to ca. 700 ka, finding that fossilized brachiopods record a similar magnitude of change in δ^7Li_{sw} as foraminifers. These results are the first to corroborate the ~9‰ increase in Cenozoic δ^7Li_{sw} and open possibilities for generating robust records of δ^7Li_{sw} in deep time, prior to foraminifer evolution.

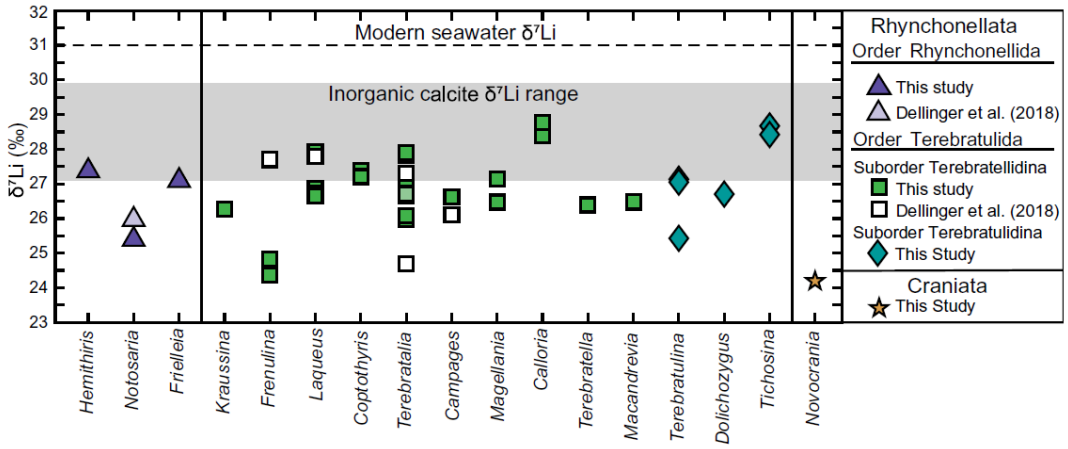

Figure 1. Modern brachiopod δ^7Li values by genus. Analytical error for all δ^7Li values is ±1‰. Gray shaded area is the δ^7Li range expected for synthetic calcite formed from seawater (Marriott et al., 2004b).

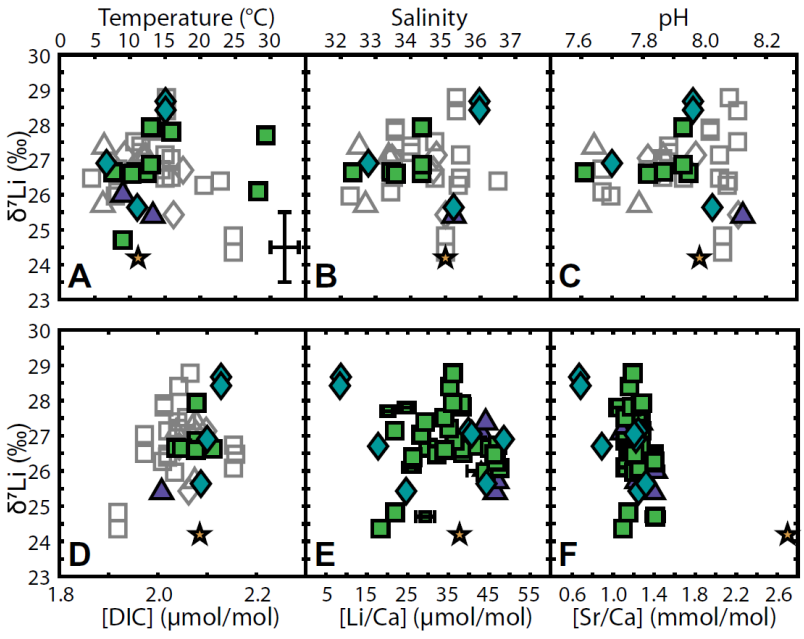

Figure 2. Relationships between brachiopod δ^7Li and estimated environmental conditions: temperature **a**, salinity **b**, pH **c**, dissolved inorganic carbon (DIC) concentration **d**, and sample Li/Ca e and Sr/Ca ratios **f**. Symbols match phylogenies in Figure 1. Open symbols are specimens lacking depth data (see text). Vertical error bars in panel A represent 2σ uncertainty for δ^7Li values, and horizontal error bars represent estimated temperature uncertainty. Error bars in panel E represent the relative standard

deviation (%) for Li/Ca values from Dellinger et al. (2018). Errors for all other measurements are smaller than the symbols. Data from Dellinger et al. (2018) are included where available.

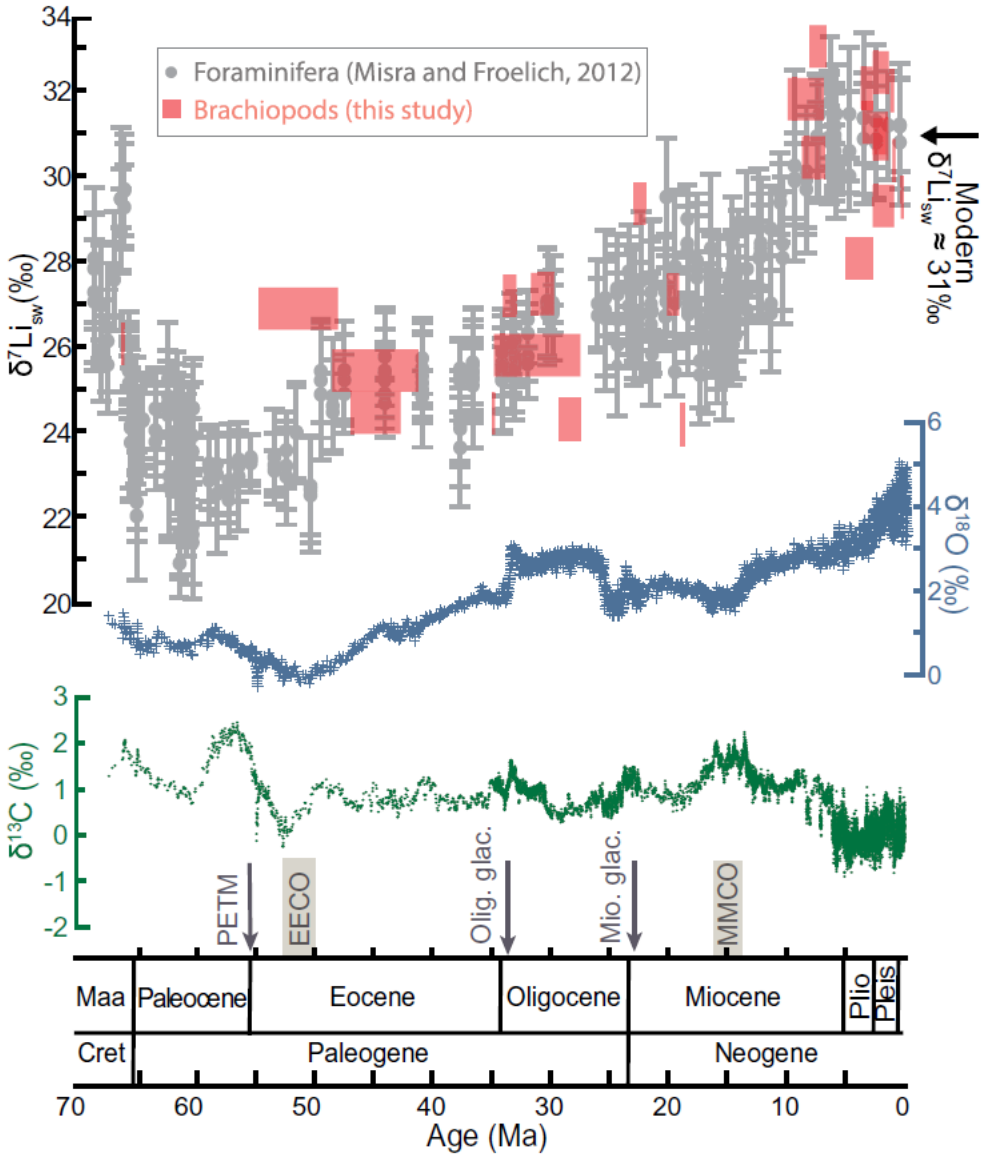

Figure 3. Seawater δ^7Li (δ^7Li_{sw}) values over the past ~70 m.y. from new brachiopod data (this study) and published foraminifer data (Misra and Froelich, 2012), after adjusting for fractionation (see Fig. S8 [see footnote 1]). Rectangle widths are ages from stratigraphy and $^{87}Sr/^{86}Sr$ values; heights reflect δ^7Li 1σ analytical uncertainty. Gray error bars represent 2σ uncertainty for replicate foraminfer δ^7Li measurements. Also shown are $\delta^{18}O$ and $\delta^{13}C$ records from benthic foraminifers (Zachos et al., 2001), reflecting climate and carbon cycle change over this time, respectively. Climatic events: PETM—Paleocene-Eocene Thermal Maximum; EECO—Early Eocene Climatic Optimum; Olig. glac.—Oligocene glaciation; Mio. glac.—Miocene glaciation; MMCO—Mid-Miocene Climatic Optimum. Cret—Cretaceous; Maa—Maastrichtian; Plio—Pliocene; Pleis—Pleistocene.

3. 西藏南部上地幔及超钾质岩浆的氧化还原状态

翻译人：冯婉仪 fengwy@sustech.edu.cn

Li W K, Yang Z M, Chiaradia M, et al. ***Redox state of southern Tibetan upper mantle and ultrapotassic magmas*** *[J].* ***Geology****, 2020, https://doi.org/10.1130/G47411.1.*

摘要：在一些构造环境中的上地幔（如：克拉通地幔、大洋地幔和岩浆弧下的地幔楔）的氧化还原状态已被很好地记录下来。相比之下，全球造山带之下的上地幔的氧逸度（fO_2）数据较少，并且决定造山带之下的上地幔 fO_2 状态的机制没有得到很好的约束。本文研究了来自喜马拉雅造山带之下西藏南部岩石圈地幔的地幔捕虏体以及含有这些捕虏体的后碰撞超钾质火山岩的 fO_2。地幔捕虏体的 fO_2 范围为 ΔFMQ = +0.5 ~ +1.2（其中 ΔFMQ 是铁橄榄石-磁铁矿-石英缓冲 fO_2 对数偏差），这表明西藏南部岩石圈地幔比克拉通地幔和大洋地幔更为氧化，并且它落入典型的地幔楔 fO_2 范围。矿物学证据表明，从俯冲的新特提斯大洋板片和印度大陆板块中释放出来的富水流体和沉积物熔体导致了西藏南部的岩石圈地幔的氧化。超钾质岩浆的 fO_2 条件显示岩浆在上升过程中会变得更氧化（ΔFMQ 从+0.8 变为+3.0）。地壳演化过程（如：分离结晶）可能影响岩浆的 fO_2，因此幔源岩浆的氧化还原状态可能并不仅仅代表其地幔源区的氧化还原状态。

ABSTRACT: The redox state of Earth's upper mantle in several tectonic settings, such as cratonic mantle, oceanic mantle, and mantle wedges beneath magmatic arcs, has been well documented. In contrast, oxygen fugacity (fO_2) data of upper mantle under orogens worldwide are rare, and the mechanism responsible for the mantle fO_2 condition under orogens is not well constrained. In this study, we investigated the fO_2 of mantle xenoliths derived from the southern Tibetan lithospheric mantle beneath the Himalayan orogen, and that of postcollisional ultrapotassic volcanic rocks hosting the xenoliths. The fO_2 of mantle xenoliths ranges from ΔFMQ = +0.5 to +1.2 (where ΔFMQ is the deviation of log fO_2 from the fayalite-magnetite-quartz buffer), indicating that the southern Tibetan lithospheric mantle is more oxidized than cratonic and oceanic mantle, and it falls within the typical range of mantle wedge fO_2 values. Mineralogical evidence suggests that water-rich fluids and sediment melts liberated from both the subducting Neo-Tethyan oceanic slab and perhaps the Indian continental plate could have oxidized the southern Tibetan lithospheric mantle. The fO_2 conditions of ultrapotassic magmas show a shift toward more oxidized conditions during ascent

(from ΔFMQ = +0.8 to +3.0). Crustal evolution processes (e.g., fractionation) could influence magmatic fO_2, and thus the redox state of mantle-derived magma may not simply represent its mantle source.

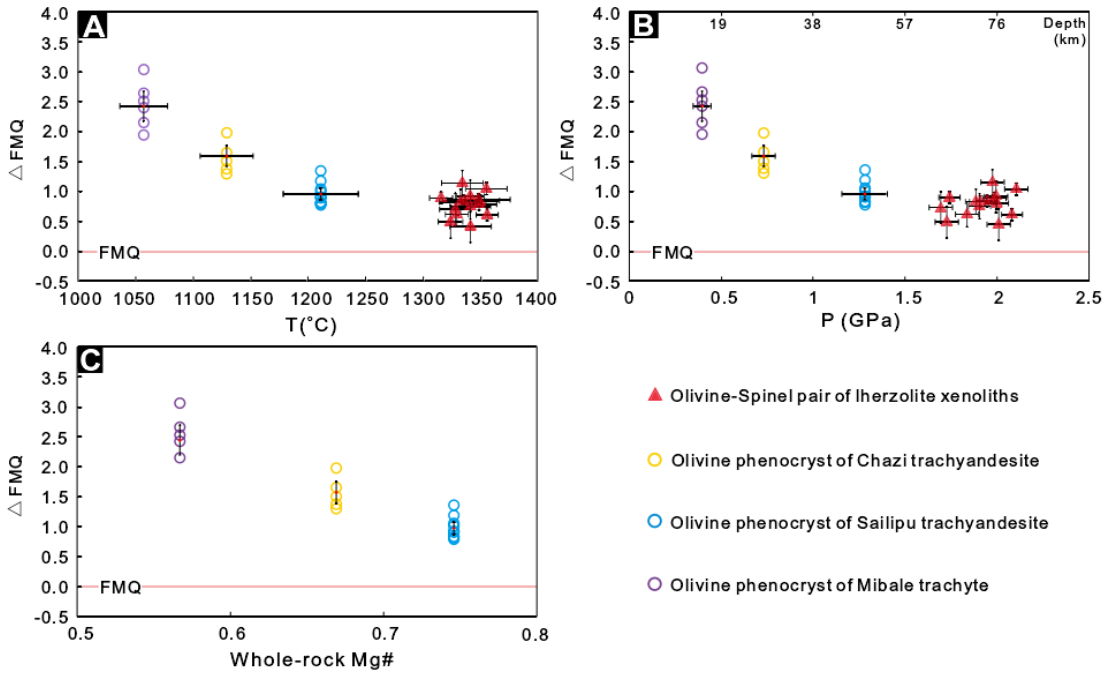

Figure 1. (A) ΔFMQ versus temperature (T), (B) ΔFMQ versus pressure (P), and (C) ΔFMQ versus whole-rock Mg#, where ΔFMQ is the deviation of log fO_2 from the fayalite-magnetitequartz buffer. Error bars of lherzolite xenoliths are calculated errors of ΔFMQ, T, and P. For results of olivines in ultrapotassic volcanic rocks (UVRs; unfilled circles), only one crossed error bar was added to average-value position of each data group to represent average error. Data sources are given in Tables S1–S3 and S5 (see footnote 1).

4. 新西兰 Hikurangi 俯冲边缘的变形前缘附近的一个逆冲断层的应变分配：IODP 的 375 航次 U1518 钻孔的磁组构研究

翻译人:李园洁 liyj3@sustech.edu.cn

Greve A, Kars M, Zerbst L, et al. ***Strain partitioning across a subduction thrust fault near the deformation front of the Hikurangi subduction margin, New Zealand: A magnetic fabric study on IODP Expedition 375 Site U1518[J]. Earth and Planetary Science Letters****, 2020, 542: 116322. doi:10.1016/j.epsl.2020.116322*

摘要:了解主动增生系统的逆冲断层和张性断层的应变分布对理解沉积物的力学性质以及断裂带的强度及其滑动行为至关重要。本文利用磁化率各向异性（AMS）技术研究沉积压实和构造发育在 Papaku 断层的应变分布，该断层是新西兰 Hikurangi 俯冲边缘的变形前缘附近的一个张性断层。国际大洋发现计划（IODP）钻孔 U1518 钻到断层上盘，断裂带和断层下盘的序列，最深到海底下 484.9 米。共 333 个离散样品进行了 AMS 测量和剩磁测量用来重建地理参考框架中每个样品的轴向方向。AMS 结果显示上盘到断裂带到下盘具有明显的组构差异，证明应变沿着断裂带分配。上盘的序列表现出 K_{max} 为一条平行于走向东北向的线，呈扁长形，东北-南西横向缩短。相比之下，下盘序列更扁圆，并在超北方向上 K_{max} 聚类。这表明下盘应变以重力载荷为主，但存在平行于太平洋板块汇聚方向的水平东西方向的应变。上盘和下盘序列之间的应变解耦发生在 Papaku 断层的顶部附近。混入断裂带的下盘沉积物和之下未变形的下盘序列之间的磁化率的差异表明欠固结的下盘序列逐步脱水。

ABSTRACT: Understanding the distribution of strain along thrust and splay faults in active accretionary systems is crucial to understand the mechanical properties of the sediments and the strength of the fault zone and its slip behavior. This paper investigates the distribution of strain through sediment compaction and texture development across the Papaku fault, a major splay fault near the deformation front of the Hikurangi subduction margin, New Zealand using the anisotropy of magnetic susceptibility technique (AMS). International Ocean Discovery Program Site U1518 penetrated hanging wall, fault zone and footwall sequences to a maximum depth of 484.9 meters below seafloor. A total of 330 discrete samples was subjected to AMS measurements and magnetic remanence data used to reconstruct the axial orientation of each sample in a geographic reference frame. The AMS display distinct fabric differences between hanging wall, through the fault zone and footwall domains, demonstrating that strain is partitioned across the fault zone. Hanging wall sequences show a strike-parallel northeasterly lineation of Kmax and weakly prolate shapes, typical

for a component of northeast-southwest lateral shortening. In contrast, footwall sequences are more oblate and show a clustering of Kmax in northerly direction. This demonstrates that strain in the footwall is dominated by gravitational loading, however a component of sub-horizontal east-westerly strain, parallel to the convergence direction of the Pacific Plate exists. Strain decoupling between hanging- and footwall sequences occurs near the top of the Papaku fault zone. Differences in the degree of magnetic susceptibility between footwall sediments incorporated into the fault zone, and the underlying undeformed footwall sequences are indicative for the progressive dewatering of the underconsolidated footwall sequences.

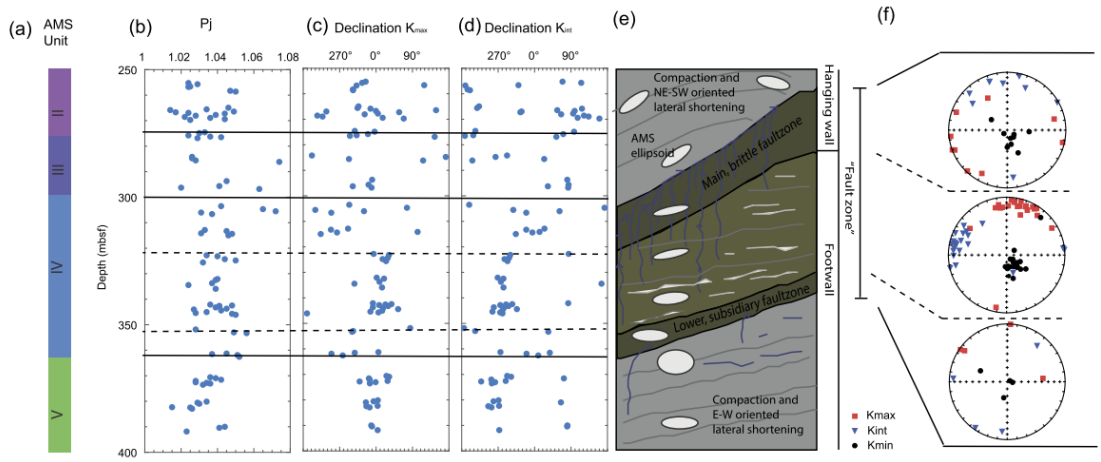

Figure 1. Downhole variations in (a) AMS units, (b) the corrected degree of anisotropy Pj, (c) the declination of K_{max}, (d) the declination of K_{int} in core-coordinates and (f) the distribution of the three principal axes of magnetic susceptibility for the upper strand of the Papaku fault zone between 304.5 and 322.4 mbsf, the center of the fault zone between 322.4 and 351.2 mbsf, and the lower strand of the Papaku fault zone between 351.2 and 361.7 mbsf. (e) Conceptual model of fault zone deformation and dewatering discussed in this paper.

5. 一个分层（stratified layer）内的磁场增强

翻译人：柳加波

Hardy C M, Livermore P W, Niesen J. ***Enhanced magnetic fields within a stratified layer[J]****. Geophysical Journal International, 2020.*

https://doi.org/10.1093/gji/ggaa260

摘要：大量关于地核构成的地震学和数值实验证据表明，在地球外核的顶部存在一层稳定的流体分层。在这个分层中，磁扭曲力平衡和受限的径向运动导致磁场收到严格限制，也就是 Malkus 约束。Malkus 约束是对众所周知的 Taylor 约束更为严格的扩展。本文，我们探讨了这种约束对地核内部磁场结构的影响。我们提供了 Malkus 约束的简单推导，并且展示了存在可以用来匹配具有任意深度的分层的任意外部势场的解。仅考虑静磁 Malkus 约束，是不可能从外部地磁观测中得到分层的唯一深度。我们研究了定义在球形地核内两个地磁场模型，它们在内部对流区域服从 Taylor 约束，在外部分层中服从 Malkus 约束。当与单个时间点的地磁势场模型匹配，这个两个模型都表明，外层内部的环形磁场强度是内部区域的约 100 倍，最大值 8mT 位于 70km 深度。因此，由受限的径向运动以及局部增强的地磁场调节的这种分层的变化机制，可能与任何内部发电机模型都截然不同。

ABSTRACT： Mounting evidence from both seismology and numerical experiments on core composition suggests the existence of a layer of stably stratified fluid at the top of Earth's outer core. In such a layer, a magnetostrophic force balance and suppressed radial motion lead to stringent constraints on the magnetic field, named Malkus constraints, which are a much more restrictive extension of the well known Taylor constraints. Here, we explore the consequences of such constraints for the structure of the core's internal magnetic field. We provide a new simple derivation of these Malkus constraints, and show solutions exist which can be matched to any external potential field with arbitrary depth of stratified layer. From considerations of these magnetostatic Malkus constraints alone, it is therefore not possible to uniquely infer the depth of the stratified layer from external geomagnetic observations. We examine two models of the geomagnetic field defined within a spherical core, which obey the Taylor constraints in an inner convective region and the Malkus constraints in an outer stratified layer. When matched to a single-epoch geomagnetic potential field model, both models show that the toroidal magnetic field within the outer layer is about 100 times

stronger compared to that in the inner region, taking a maximum value of 8 mT at a depth of 70 km. The dynamic regime of such a layer, modulated by suppressed radial motion but also a locally enhanced magnetic field, may therefore be quite distinct from that of any interior dynamo.

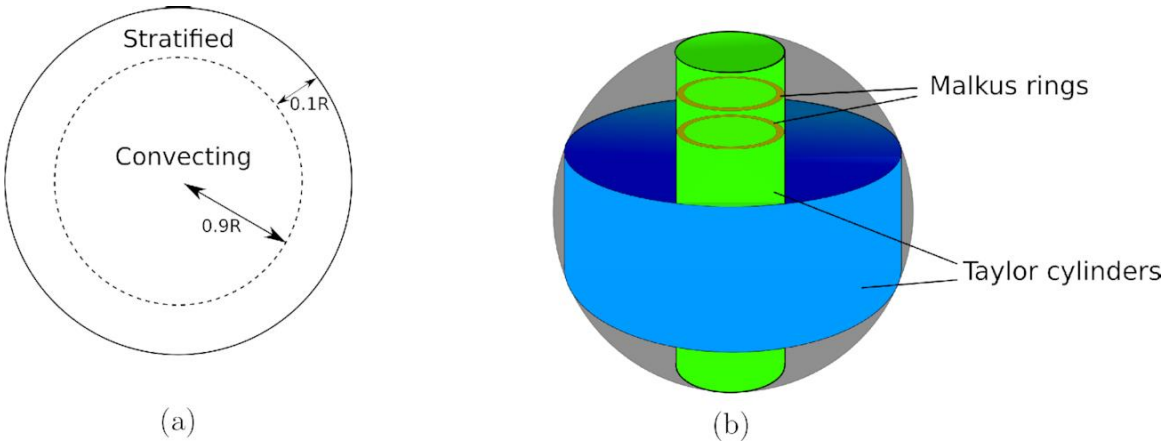

Fig 1: (a) Earth-like spherical shell with radius r_{SL} = 0.9R. A Malkus state defined in a stratified layer surrounds an interior Taylor state. (b) Geometry of constraint surfaces.

6. 菲律宾海板块印度洋型同位素特征的出现:来自早白垩世地体的 Hf 和 Pb 同位素证据

翻译人：刘伟 inewway@163.com

Hickeyvargas R, Bizimis M, Deschamps A, et al. ***Onset of the Indian Ocean isotopic signature in the Philippine Sea Plate: Hf and Pb isotope evidence from Early Cretaceous terranes****[J]. Earth and Planetary Science Letters, 2008, 268(3): 255-267. https://doi.org/10.1016/j.epsl.2008.01.003*

摘要：菲律宾板块弧后盆地内古新世至今的玄武岩具有印度洋型洋中脊玄武岩（MORB）的 Pb、Hf 和 Nd 同位素特征。我们通过对菲律宾海板块早白垩世地体同位素组成的研究，来理解印度洋型 MORB 同位素信号的出现和起源。花东盆地是早白垩世海洋岩石圈的一部分，与古新世-渐新世西菲律宾盆地相连接，其岩石具有印度洋型 MORB 的 Hf-Nd 同位素特征，但 Pb 同位素值介于印度洋型和太平洋型 MORB 之间。西菲律宾盆地玄武岩相较花东盆地具有较强的印度洋型 Pb 同位素特征。Amami 高原火成岩俯冲前的地幔源具有太平洋型 MORB 的同位素特征，俯冲组分具有太平洋型 MORB 和沉积物混合的同位素特征。花东盆地早白垩世岩石的印度洋型 MORB 特征指示具有这种特征的地幔源在今天的印度洋形成之前就存在了，现在整个欧亚大陆南部发现的特提斯大洋玄武岩也具有这一特征。随着西菲律宾盆地的打开，其玄武岩具有比花东盆地圈闭的老玄武岩更明显的印度洋型 Pb 同位素特征。Amami 高原的结果指示菲律宾海板块也包含太平洋型岩石圈，可能分布在俯冲地块，如菲律宾群岛，其在西菲律宾海盆地打开的过程中分裂。综合结果表明，古 IBM 弧形成的岩石圈是多样的，包括太平洋型和印度洋型岩石圈，以及古老、亏损的俯冲条件下的弧幔楔。

ABSTRACT: Basalts from Paleocene–recent back arc basins within the Philippine Sea Plate have the Pb and Hf–Nd isotopic characteristics of Indian Ocean mid-ocean ridge basalts (MORB). We examined the isotopic composition of rocks from Early Cretaceous terranes within the Philippine Sea Plate, in order to understand the onset and origin of the Indian MORB isotopic signal. Igneous rocks from the Huatung Basin, a fragment of Early Cretaceous oceanic lithosphere sutured to the Paleocene–Oligocene West Philippine Basin, have an Indian MORB Hf–Nd isotopic signature, but Pb isotope ratios are intermediate between those of Indian and Pacific MORB. West Philippine Basin basalts have a stronger Indian Pb isotope signature than Huatung Basin rocks. Pre-subduction mantle sources for igneous rocks from the Amami Plateau, an Early Cretaceous island arc in the northernmost Philippine Sea Plate, have isotopic characteristics of Pacific MORB, and subducted

components added to the mantle sources also have isotopic characteristics of Pacific MORB, plus sediment.

The Indian MORB characteristics of Early Cretaceous Huatung Basin rocks lend support to the idea that mantle sources with this signature existed prior to the opening of the present day Indian Ocean and that Tethyan oceanic basalts, now found throughout southern Eurasia, shared them. As the West Philippine Basin opened, basalts formed from mantle sources with a more pronounced Indian Pb isotope signature than those tapped by the older Huatung Basin. Results for the Amami Plateau indicate that the Philippine Sea Plate also contains Pacific-type lithosphere, perhaps scattered within subduction terranes, such as the Philippine Islands, that were disrupted by basin opening. Taken together, results indicate that the lithosphere on which the proto-Izu-Bonin-Mariana arc formed was diverse, containing Pacific and Indian oceanic lithosphere, and old, depleted and subduction-conditioned arc mantle wedge.

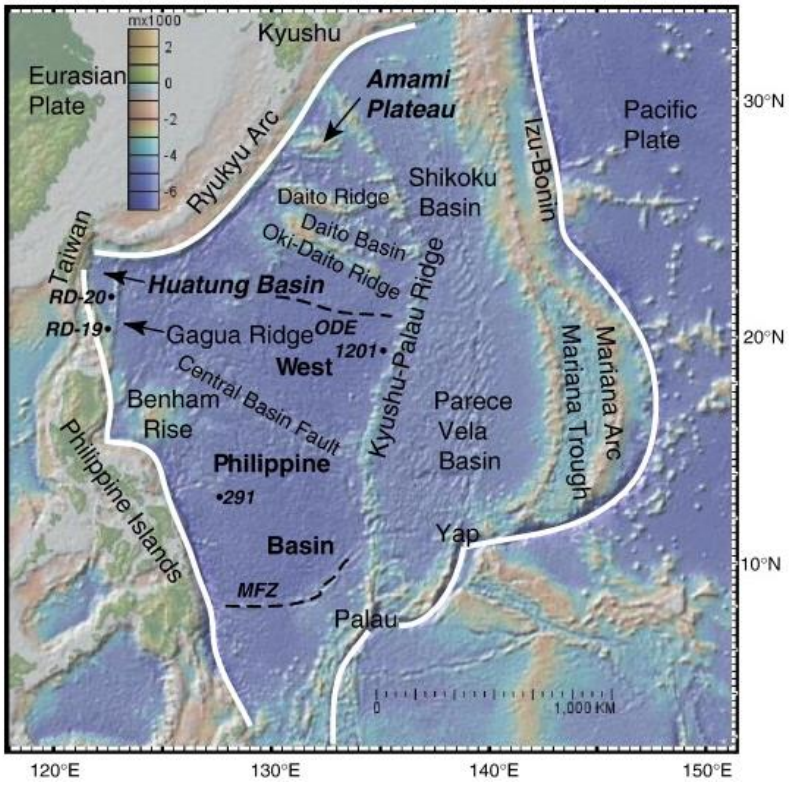

Figure 1. Map of the Philippine Sea Plate showing locations mentioned in the text. The boundaries of the Philippine Sea Plate are outlined in white. Dots with numbers are dredge and drill sites mentioned in the text. ODE is the Oki Daito Escarpment (Okino et al., 1999) and MFZ is the Mindanao Fracture Zone (Taylor and Goodliffe, 2004). The map was constructed using GeoMapApp (http://www.marine-geo.org/geomapapp/).

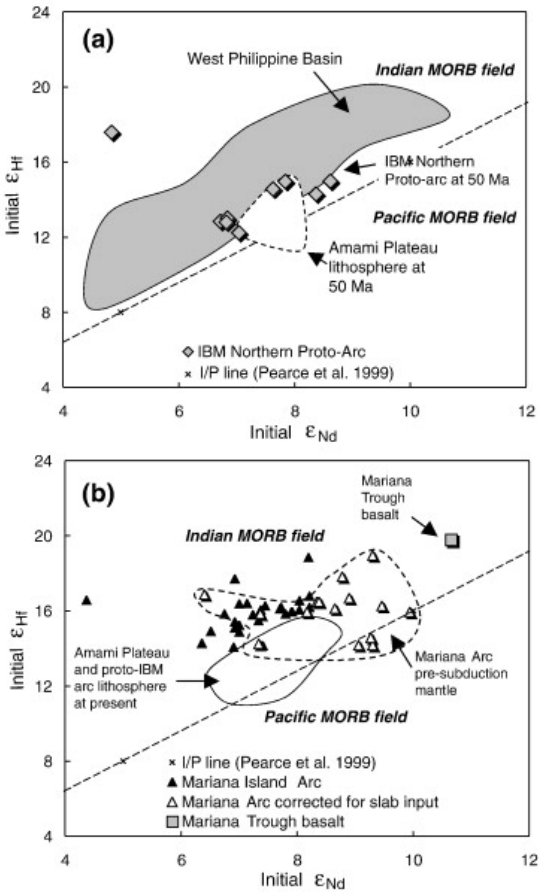

Figure 2. Plots of initial εHf versus initial εNd. In a) the range of isotope values for volcanic rocks from the Paleocene proto-Izu-Bonin-Mariana arc (Pearce et al., 1999) are compared with the field for igneous rocks from the Early Cretaceous Amami Plateau, corrected to 50 Ma, and basalts from the West Philippine Basin, as potential mantle sources. In b) Hf–Nd isotope data for the active Mariana Island (closed triangles), corrected for subduction input (open triangles), are compared with the field for older arc lavas (both proto-IBM and Amami Plateau, corrected to the present day), and basalt from the Mariana Trough. Mariana Arc and Trough data are from Woodhead et al. (2001).

7. 东亚降雨氧同位素的正偏指示区域气候和西风带的夏季季节性减弱

翻译人：杨会会 11849590@mail.sustech.edu.cn

Chiang J C H, Herman M J , Yoshimura K et al. ***Enriched East Asian oxygen isotope of precipitation indicates reduced summer seasonality in regional climate and westerlies [J].Proceedings of National Academy of sciences of the united states of America,*** *2020, 117, 26:14745-14750*

http://www.pnas.org/cgi/doi/10.1073/pnas.1922602117

摘要：东亚地区的洞穴氧同位素记录显示，在过去的几十万年里，古气候明显发生了巨大而迅速的变化。然而，就区域气候和环流而言，同位素变化实际上代表了什么还存在争议。通过分析东亚地区降水 $\delta^{18}O$ 组成的经过雨量加权的年际变化，再用一个受大尺度大气再分析场限制的同位素模型进行模拟，我们提出一个答案。与降雨同位素和大规模大气环流有关的 $\delta^{18}O$ 正偏的年份，夏季的季节性减弱。变化发生在 6-10 月份，在这段时间里降水的 $\delta^{18}O$ 组成($\delta^{18}O_p$)从同位素上较重的冬季过渡到较轻的夏季。在 $\delta^{18}O$ 偏正的年份，这种转变不那么明显。仅靠降水量的变化不足以解释 $\delta^{18}O$ 正偏和负偏年份间雨量加权 $\delta^{18}O_p$ 的年际变化。夏季季节性的减弱也表现在低空季风南风带和高空西风带；对于后者，在夏季越过青藏高原的北移则不那么明显。因此，我们的研究结果表明，横跨高原的西风带是东亚古气候迅速变化的直接原因，调节夏季高峰的变化。（译文有些拗口，感兴趣的读者请移步原文）

ABSTRACT: Speleothem oxygen isotope records over East Asia reveal apparently large and rapid paleoclimate changes over the last several hundred thousand years. However, what the isotopic variation actually represent in terms of the regional climate and circulation is debated. We present an answer that emerges from an analysis of the interannual variation in amount-weighted annual $\delta^{18}O$ of precipitation over East Asia as simulated by an isotope-enabled model constrained by large-scale atmospheric reanalysis fields. ^{18}O-enriched years have reduced summer seasonality both in terms of precipitation isotopes and in the large-scale circulation. Changes occur between June and October, where the $\delta^{18}O$ of precipitation ($\delta^{18}O_p$) transitions from the isotopically heavier winter to the lighter summer regime. For ^{18}O-enriched years, this transition is less pronounced. Variations in precipitation amount alone are insufficient to explain the amount-weighted annual $\delta^{18}O_p$ between ^{18}O-enriched and ^{18}O-depleted years. Reduced summer seasonality is also expressed in the low-level monsoonal southerlies and upper-level westerlies; for the latter, the northward migration across the Tibetan Plateau in the summer is less pronounced. Our result thus implicates the westerlies across the plateau as the proximate cause of East Asian paleomonsoon changes, manifested as a modulation of its summer peak.

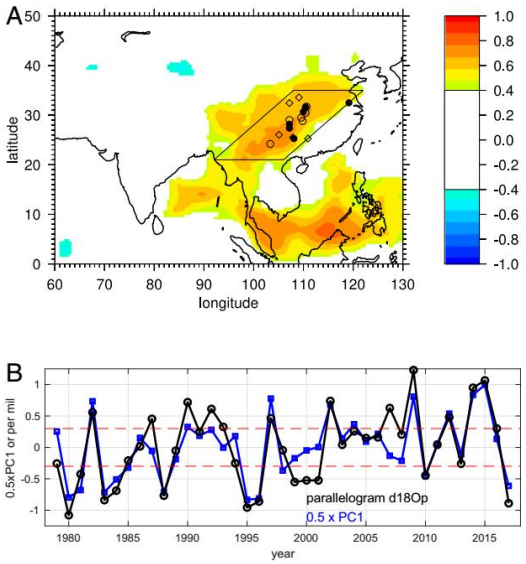

Figure 1. (A) First EOF of normalized amount-weighted annual $\delta^{18}O_p$, taken over 60 °E to 130°E and 0°N to 50°N. The dots reference locations of speleothem records; the black filled dots are the key speleothem records of Hulu, Dongge, and Sanbao, sites with excellent coherence to these records (Sanbao: 110.43°E, 31.67°N; Heshang: 110.42°E, 30.45°N; Hulu: 119.17°E, 32.5°N; Dongge: 108.08°E, 25.28°N; Haozhu: 109.98°E, 30.68°N; Shigao: 107.17°E, 28.18°N; Sanxing: 107.18°E, 27.37°N). Caves sites with good and fair coherence with the Hulu–Dongge–Sanbao record are shown as open circles and open diamonds, respectively. See SI Appendix, section 3 for a list of these records, method of comparison, and references. The parallelogram marks the region used to generate an interannual index of amount weighted annual $\delta^{18}O_p$ and encompasses the region with large EOF1 loading and location of caves sites. The vertices of the parallelogram are at (counterclockwise from the bottom left point) 92°E, 21°N; 106°E, 21°N; 122°E, 35°N; 108°E, 35°N. (B) Principal component (PC) time series of the first EOF scaled by 1/2 (blue) and average of amount-weighted annual $\delta^{18}O_p$ (units: per mil) across the parallelogram region with the mean removed (black). Dashed red lines indicate ±0.5 standard deviation. Black dots beyond these limits represent years comprising the enriched (n = 13; above) and depleted (n = 12; below) composites. The correlation coefficient between the two time series is r = 0.87 (P < 0.01)

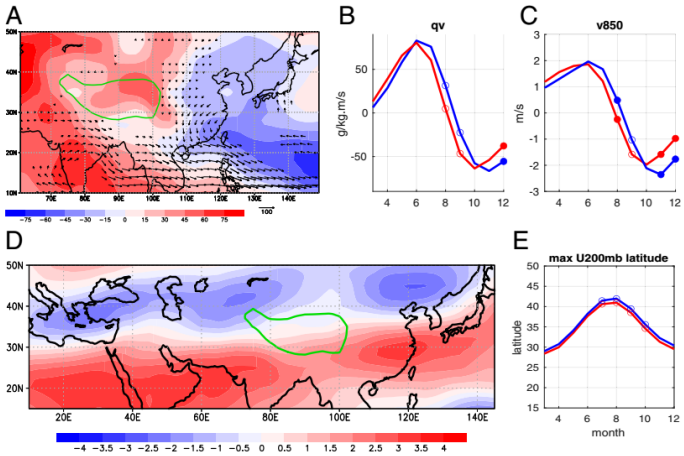

Figure 2. Seasonal changes in the atmospheric circulation. (A) The enriched minus depleted difference in JJASO vertically integrated moisture flux (vectors) and mean sea level pressure (shaded, in Pa). The green contour is the climatological 700 mb surface pressure contour, denoting the location of the Tibetan

Plateau. Only vectors for which either the zonal or meridional component is significant at $P < 0.1$ are plotted. (B) Vertically integrated meridional moisture flux averaged over 105°E to 120°E, 20°N to 30°N for enriched (red) and depleted (blue) years (in kg/[m s]). (C) Same as B, but for meridional wind at 850 mb (in m/s). (D) JJASO 200 mb zonal wind, enriched minus depleted years (in m/s). (E) Latitude of maximum jet speed across Asia centered on the plateau (40°E to 140°E) for enriched (red) and depleted (blue) years. Note that the y axis latitude range matches that for D. For B, C, and E, the time series was filtered to remove month-to-month noise prior to compositing (SI Appendix, section 4). Open circles indicate the difference between enriched and depleted years is significant at $P < 0.05$, and filled circles indicate the difference is significant at $P < 0.01$.

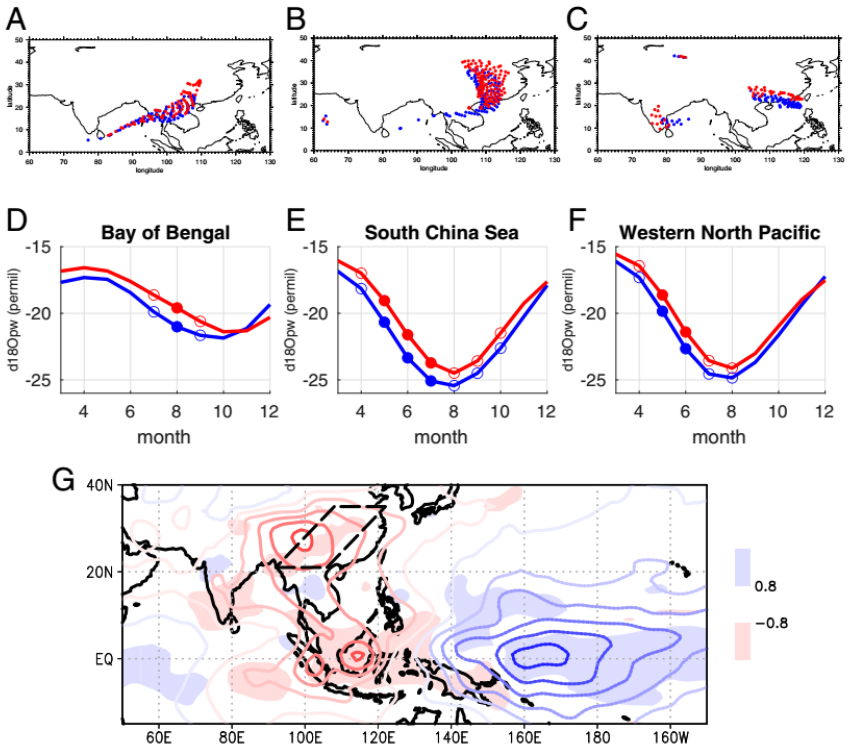

Figure 3. (A) July origins of trajectories that terminate in the parallelogram region at the 700 mb level, as calculated using a 7 d back trajectory, for enriched years (red) and depleted years (blue). (B and C) Same as A, but for August and September, respectively. (D) $\delta^{18}O_{pw}$ values averaged over the Bay of Bengal (85°E to 95°E, 10°N to 20°N) for enriched (red) and depleted (blue) years. Open circles indicate the difference between enriched and depleted years is significant at $P < 0.05$, and filled circles indicate the difference is significant at $P < 0.01$. (E and F) Same as D, but for the South China Sea (108°E to 118°E, 12°N to 22°N) and western North Pacific (118°E to 128°E, 18°N to 28°N), respectively. For D, E, and F, time series were denoised to remove month-to-month noise prior to compositing (SI Appendix, section 4). (G) JJASO rainfall changes (shaded), enriched minus depleted, and JJASO $\delta^{18}O_{pw}$ enriched minus depleted (contours). The contour interval is 0.5 per mil, and negative values are dashed. The parallelogram region is marked by the black dashed line for reference.

8. 早期火星高地重建揭示的厚地壳块体

翻译人：曹伟

Bouley S, Keane J T, Baratoux D, et al. ***A thick crustal block revealed by reconstructions of early Mars highlands****[J].* ***Nature Geoscience****, 2020, 13(2): 1-5. https://doi.org/10.1038/s41561-019-0512-6*

摘要：火星的全球规模地壳结构是由撞击盆地，火山区以及两个半球组成，包括北部低地的薄地壳和南部高地的厚地壳。南部高地通常被认为是具有共同起源和共同地质历史的古地壳形成的连贯地形，可能是由一次巨大的撞击或半球规模的地幔上涌引起的。过去的研究已经量化了火山作用对地壳结构的影响；然而大型撞击的影响目前仍然不清楚。本文中我们展示了火星过去地壳厚度的重建(大约 4.2 Gyr 前)，该重建假设质量守恒，同时移除了四个最大的撞击盆地(Hellas, Argyre, Isidis 和 Utopia)，以及主要的 Tharsis and Elysium 火山区。尽管地壳的二分现象持续存在，我们的重建显示地壳厚度的变化比目前更加缓和。然而，我们的重建揭示了与地球化学和磁异常相关的南部高地上不连续的厚地壳斑块。该区域与 Terra Cimmeria–Sirenum 相对应，被解释为一个离散的地壳块体。我们的研究结果表明，南部高地是由几个具有不同地质历史的地壳块体组成。南部高地如此复杂的结构并不能用现有的地壳形成和演化来解释

ABSTRACT：The global-scale crustal structure of Mars is shaped by impact basins, volcanic provinces, and a hemispheric dichotomy with a thin crust beneath the northern lowlands and a thick crust beneath the southern highlands. The southern highlands are commonly treated as a coherent terrain of ancient crust with a common origin and shared geologic history, plausibly originating from a giant impact(s) or a hemispheric-scale mantle upwelling. Previous studies have quantified the contribution of volcanism to this crustal structure; however, the influence of large impacts remains unclear. Here we present reconstructions of the past crustal thickness of Mars (about 4.2 Gyr ago) where the four largest impact basins (Hellas, Argyre, Isidis and Utopia) are removed, assuming mass conservation, as well as the main volcanic provinces of Tharsis and Elysium. Our reconstruction shows more subdued crustal thickness variations than at present, although the crustal dichotomy persists. However, our reconstruction reveals a region of discontinuous patches of thick crust in the southern highlands associated with magnetic and geochemical anomalies. This region, corresponding to Terra Cimmeria–Sirenum, is interpreted as a discrete crustal block. Our findings

suggest that the southern highlands are composed of several crustal blocks with different geological histories. Such a complex architecture of the southern highlands is not explained by existing scenarios for crustal formation and evolution.

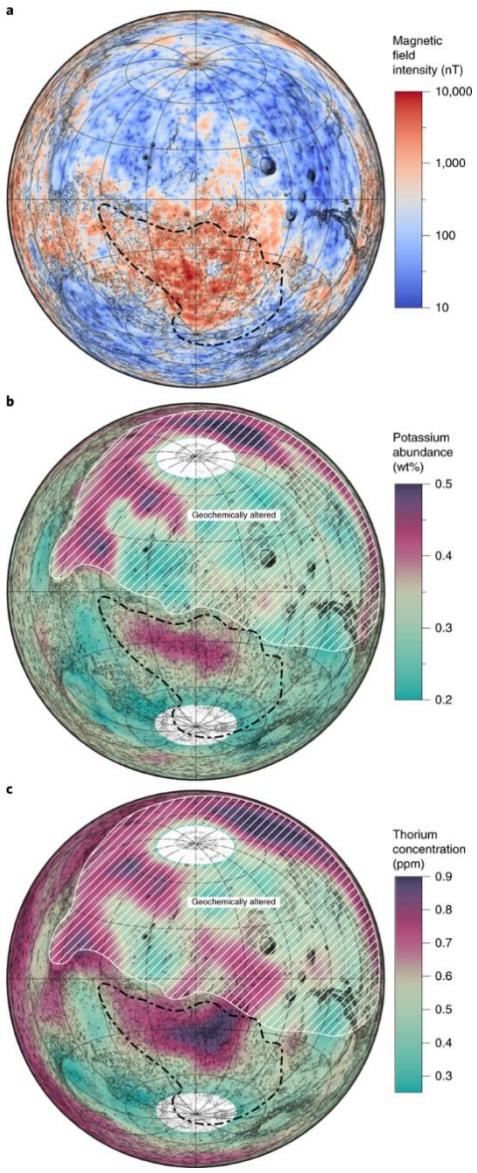

Fig. 4: The geophysical and geochemical signature of the Cimmeria–Sirenum block. a,The magnetic field intensity, evaluated at the surface of Mars. b, The potassium concentration (wt%) In b and c, the northern hemisphere is hatched out to focus attention on the signatures south of the dichotomy. The maps are in Lambert azimuthal equal-area projection, centred on 0°, and cover all of Mars except for a small region on the opposite hemisphere. The maps are overlaid on the present-day topography for reference. The Cimmeria–Sirenum crustal block is enclosed by a dash-dot line.

9. 在 Iberian 发现的早铁器时代的两个古地磁强度最大值和快速方向变化率。对 Levantine 铁器时代地磁场异常的指示

翻译人：王浩森 502691781@qq.com

Osete M L, Molina-Cardín A, Campuzano S A, et al. ***2020. Two archaeomagnetic intensity maxima and rapid directional variation rates during the Early Iron Age observed at Iberian coordinates. Implications on the evolution of the Levantine Iron Age Anomaly. Earth and Planetary Science Letters [J], 533: 116047.***

https://doi.org/10.1016/j.epsl.2019.116047

摘要：Iberian 半岛的地磁场变化在晚铁器时代之前的研究有限。本文报告了从西班牙东部六个考古遗址中得到的 17 个燃烧物进行的古地磁研究得出的 14 个定向强度和 10 个古强度结果。所研究的材料已根据考古证据确定日期，并得到放射性碳同位素年龄（公元前 8-5 世纪）。岩石磁学实验表明，剩余的磁化强度是由居里温度为 500-575°C 的低矫顽力矿物承载，最有可能是钛磁铁矿/磁铁矿，钛含量低。利用经典的 Thellier-Thellier 实验（包括 pTRM 检查和磁各向异性校正）进行古强度测定。得到了铁器时代的新的全矢量伊比利亚古强度变化曲线。并且发现在早期铁器时代在古强度方向和强度上的较高波动率，这似乎与 Levantine 铁器年龄异常（LIAA）有关，后者是近三千年来最显着的地磁场异常。在 Levantine 处观测到两个强度最大值，最古老的出现在公元前 750 年左右（与东部约 23º 的偏角相关），第二个出现了 275 年后的北方向上（公元前 475 年）。对于最早的材料（公元前 750 年），相关的虚拟轴向偶极矩最高为 $14 \cdot 10^{22} Am^2$，但是对于早期铁器时代末期的记录，相关的虚拟轴向偶极矩达到 $16 \cdot 10^{22} Am^2$。为了调查古磁场异常高的起因，我们开发了一种新的全球地磁场重建模型，即 SHAWQ-IronAge 模型，该模型基于对全球地磁和火山数据集的严格修订。新模型提供了对 LIAA 演化的改进描述，它与阿拉伯半岛下方核幔边界（CMB）上的磁通量斑块有关，在公元前 950 年左右可以清楚地观察到。该磁通量斑块向西北扩展，同时强度降低，在公元前 750 年左右到达伊比利亚。大约在公元前 600-500 年，它似乎在原地消失了，之后在欧洲大陆下面进行了重建。

ABSTRACT: Variations of geomagnetic field in the Iberian Peninsula prior to Late Iron Age times are poorly constrained. Here we report 14 directional and 10 palaeointensity results from an archaeomagnetic study carried out on 17 combustion structures recovered from six archaeological sites in eastern Spain. The studied materials have been dated by archaeological evidences and supported by radiocarbon dates (8th-5thcenturies BC). Rock magnetic experiments indicate that the

characteristic remanent magnetization is carried by a low coercivity magnetic phase with Curie temperatures of 500-575◦C, most likely titanomagnetite/maghemite with low titanium content. Archaeointensity determinations were carried out by using the classical Thellier-Thellier experiment including pTRM-checks and magnetic anisotropy corrections. A new full vector Iberian Paleosecular Variation Curve for the Iron Age is presented. High fluctuation rates on both directions and intensities are observed during the Early Iron times that seems to be related with the Levantine Iron Age Anomaly (LIAA), the most prominent anomaly of the geomagnetic field of the last three millennia. Two intensity maxima were observed at Iberian coordinates, the oldest around 750 BC (associated with easterly declinations of around 23◦) and the second 275 yrslater (475 BC) with northerly directions. The related virtual axial dipole moment was up to 14 ·1022Am2for the oldest materials (750 BC) and reaching 16 ·1022Am2for the materials corresponding to the end of the Early Iron Age. In order to investigate the origin of the unusually high fluctuations of the palaeofield we have developed a new global geomagnetic field reconstruction, the SHAWQ-IronAge model, which is based on a critical revision of the global archeomagnetic and volcanic dataset. The new model provides an improved description of the evolution of the LIAA, which is related to a normal flux patch at the core-mantle boundary (CMB) below Arabian Peninsula clearly observed at around 950 BC. This flux patch expanded towards the north-west, while decreasing in intensity, reaching Iberia at around 750 BC. Around 600-500 BC, it underwent a revival below the European continent after that it seems to vanish in situ.

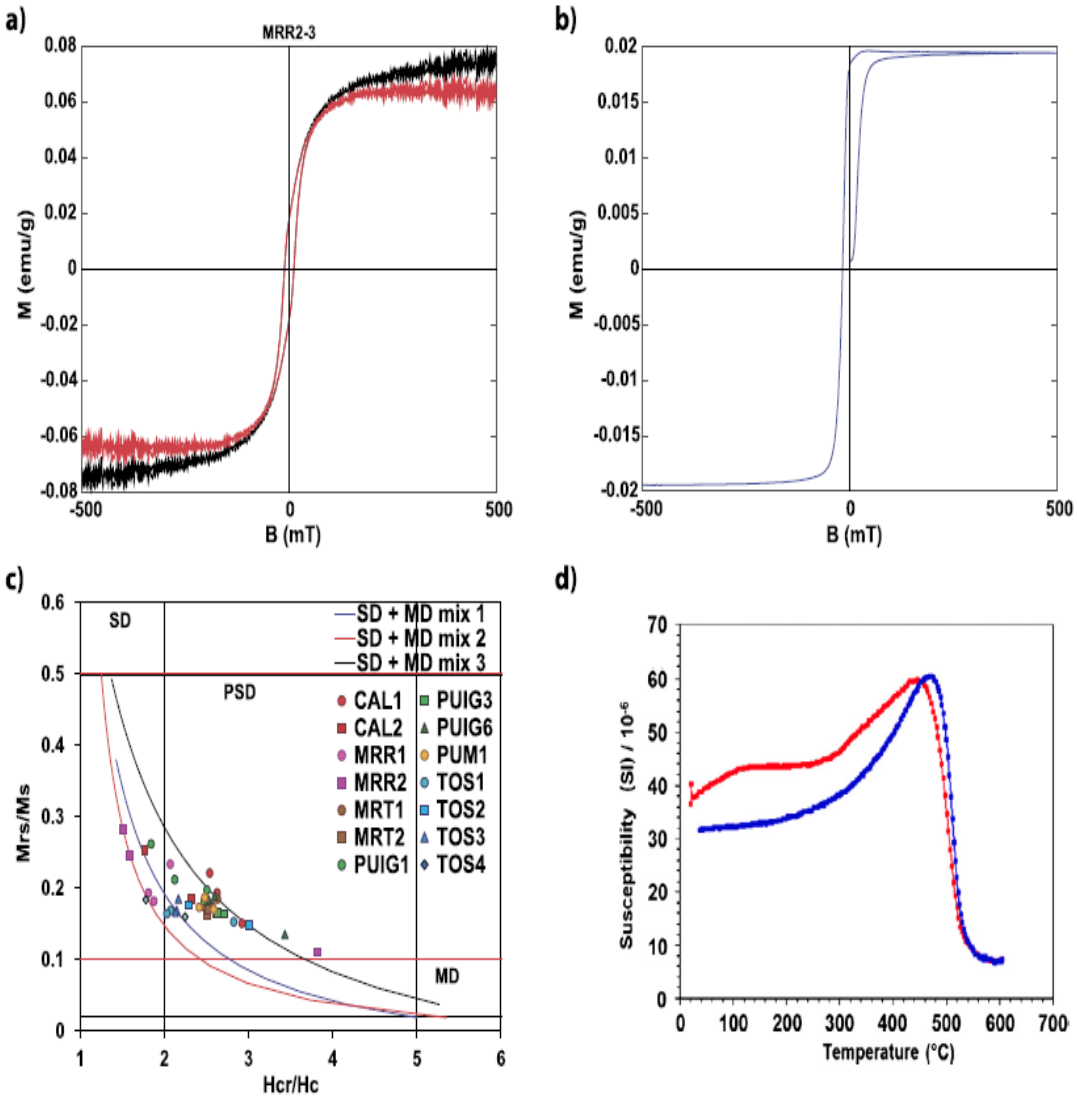

Fig.1. Representative rock-magnetic results. hysteresis curves (a) (red corrected by the paramagnetic contribution, black uncorrected), (b) SIRM and back field; (c) Day plot of hysteresis ratios; (d) Susceptibility versus temperature Heating/cooling is shown in red/blue. (For interpretation of the colours in the figure(s), the reader is referred to the web version of this article.)

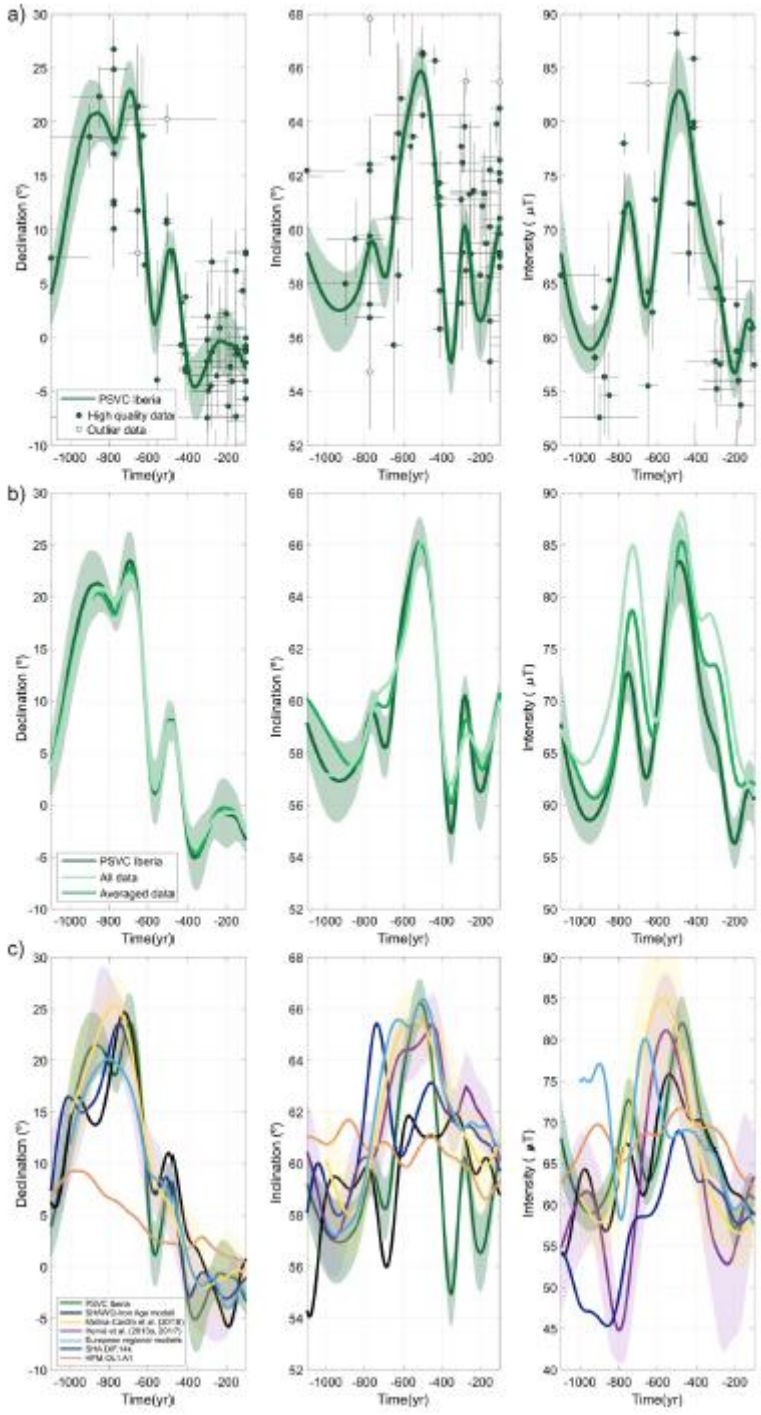

Fig.2.a) Full vector Iberian PSVC based on high quality data, together with the data used for its construction. It has been represented with a 2-sigma error band. Open circles represent the outliers rejected for curve calculation. b) Iberian palaeosecular variation curves obtained with different input datasets (dark green: only quality data, light green: all data from the database, green: all data with averages of data based on one specimen).c) Iberian PSVC compared with other curves and synthetic curves derived from regional and global models.

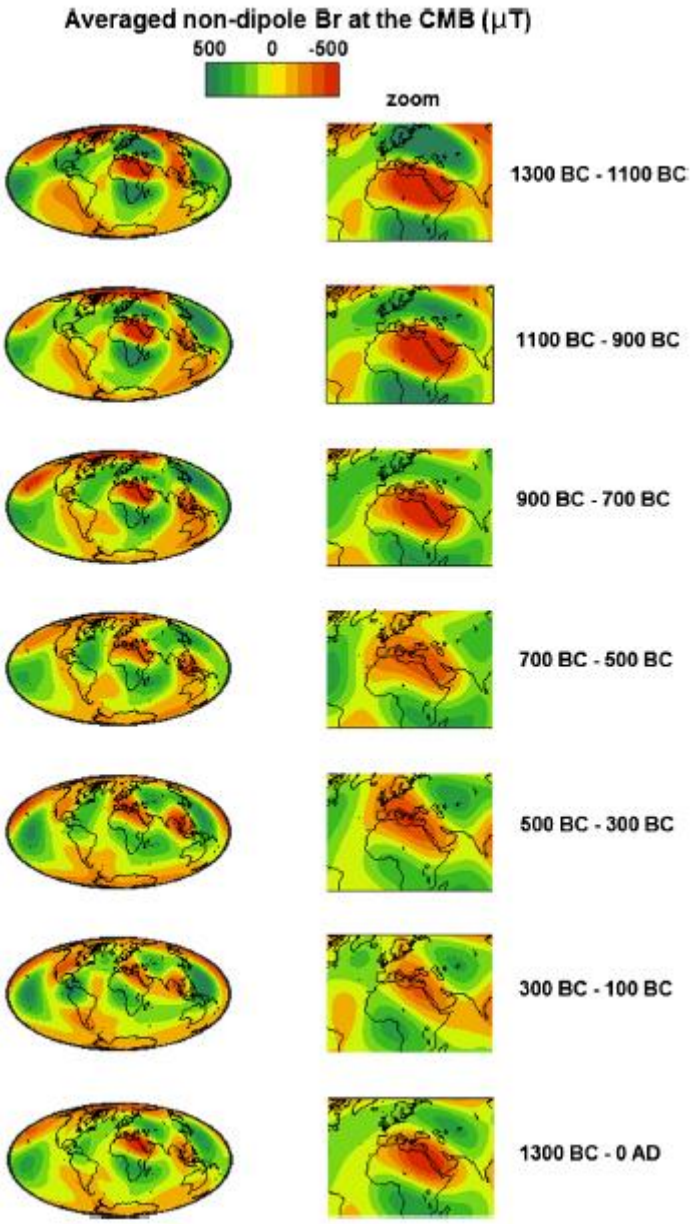

Fig.3. Evolution of non-dipole radial field at the CMB computed for the 1300 BC – 0 AD time period averaged every 200 yrsusing the SHAWQ-Iron Age model.

10. 基于单颗石藻的二次离子质谱痕量金属(Mg/Ca 和 Sr/Ca)分析

翻译人：王敦繁 dunfan-w@foxmail.com

Katy, Prentice, Tom,et. ***Trace metal (Mg/Ca and Sr/Ca) analyses of single coccoliths by Secondary Ion Mass Spectrometry[J]. Geochimica Et Cosmochimica Acta,*** *2014.*

摘要：本文首次对从单颗石中获得的现代和化石球颗石微量金属数据进行了多物种比较。我们提供了痕量金属分析(Sr、Ca、Mg 和 Al)和用二次离子质谱法(SIMS)获得的单个古近系球粒化石的分布图。我们利用这些数据来确定不同的颗石保存和成岩方解石覆盖层对记录的颗石方解石中锶和镁浓度的影响。通过对始新世/渐新世过渡的深海沉积物中的颗屑分析表明，原生颗屑方解石在相似的沉积环境中对浮游有孔虫中常见的新形态具有抗性。相反，在存在的地方，成岩方解石形成了明显的覆盖在原生颗石方解石上，而不是取代这个方解石。在 SIMS 分析中，相对于原生的颗岩方解石，相对较高的 Mg 和较低的 Sr 浓度可以很容易地区分出颗岩上的成岩覆盖。这一解释被现代培养的勃氏小球虫的可比 SIMS 分析所证实。此外，由于成岩型方解石过度生长是球粒基地球化学记录偏压的主要来源，我们推断在古跃层下沉积的碳酸盐含量较低的岩性岩性比普遍存在过度生长的富含碳酸盐的沉积物更有可能产生以初级球粒方解石为主的地球化学记录。在低碳酸盐岩性中保存原生粒碳酸盐岩提供了一个可靠的地球化学档案，那里没有浮游有孔虫或经历了新形态。

ABSTRACT: Here we present the first multi-species comparison of modern and fossil coccolith trace metal data obtained from single liths. We present both trace metal analyses (Sr, Ca, Mg and Al) and distribution maps of individual Paleogene fossil coccoliths obtained by Secondary Ion Mass Spectrometry (SIMS). We use this data to determine the effects of variable coccolith preservation and diagenetic calcite overgrowths on the recorded concentrations of strontium and magnesium in coccolith calcite. The analysis of coccoliths from deep-ocean sediments spanning the Eocene/Oligocene transition demonstrates that primary coccolith calcite is resistant to the neomorphism that is common in planktonic foraminifera from similar depositional environments. Instead, where present, diagenetic calcite forms distinct overgrowths over primary coccolith calcite rather than replacing this calcite. Diagenetic overgrowths on coccoliths are easily distinguished in SIMS analyses on the basis of relatively higher Mg and lower Sr concentrations than co-occurring primary coccolith calcite. This interpretation is confirmed by the comparable SIMS analyses of modern cultured coccoliths of Coccolithus braarudii. Further, with diagenetic calcite overgrowth

being the principle source of bias in coccolith-based geochemical records, we infer that lithologies with lower carbonate content, deposited below the palaeolysocline, are more likely to produce geochemical records dominated by primary coccolith calcite than carbonate-rich sediments where overgrowth is ubiquitous. The preservation of primary coccolith carbonate in low-carbonate lithologies thus provides a reliable geochemical archive where planktonic foraminifera are absent or have undergone neomorphism.

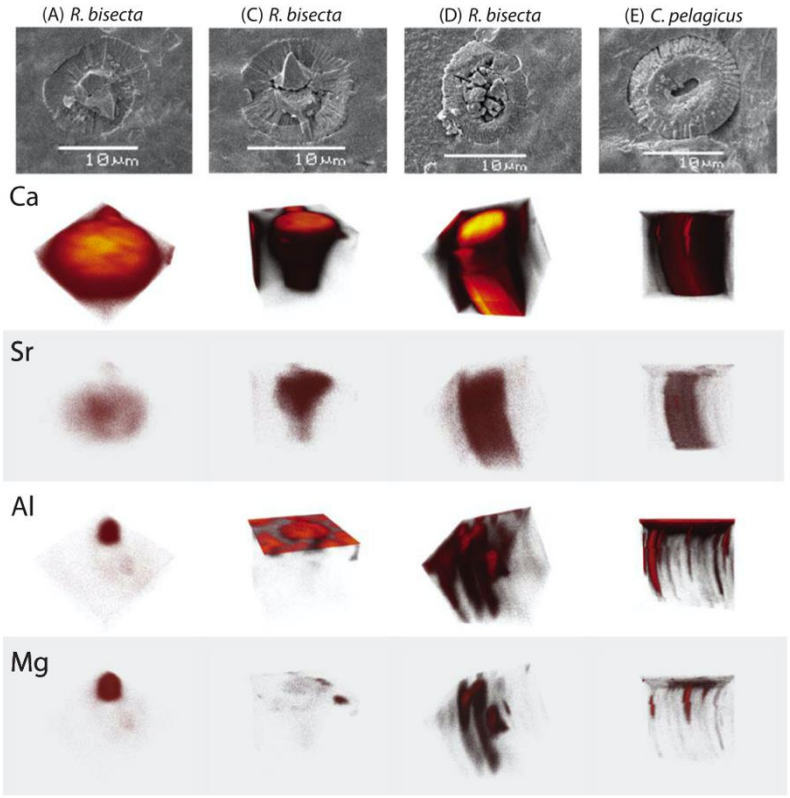

Figure 1. 3-D ion maps created using the ToF-SIMS V. Cycles are superimposed on top of each other, with hot-coloured areas representing high density of the ion selected throughout the coccolith and surrounding media. Maps for Ca, Sr, Al and Mg are shown. The coccoliths pictured are the same as those in Fig. 5 (details of each coccolith are given in Table 2). It should be noted that it is not possible to scale the specimens for their true depth as the sputter rate of coccoliths is unknown. The images therefore do not display the correct depth scale, and an arbitrary depth is used by the software in the creation of the images.

11. 探地雷达和沉积物磁化率分析在一个澳大利亚北部砂岩岩棚的探索应用

翻译人：郑威　11930589@mail.sustech.edu.cn

Lowe K M, Wallis L A. ***Exploring ground-penetrating radar and sediment magnetic susceptibility analyses in a sandstone rockshelter in northern Australia****[J].* ***Australian Archaeology****, 2020: 1-12. https://doi.org/10.1080/03122417.2020.1764172*

摘要：探地雷达为无损评估考古遗址岩棚的地层信息提供了多种便利，包括地下地层学信息和例如洞顶崩塌和基岩之类的各种要素的信息。理解澳大利亚岩棚下沉积物记录的人类活动和遗址形成过程的挑战包括：在哪进行考古发掘？如何最好地确定石器出现之后人类占领的顺序？以及如何解决关于地层关联的问题？这篇文章阐述了如何使用探地雷达更好地获取对于一个更新世岩棚下埋藏的沉积物的理解。与沉积物磁化率研究结果对比，探地雷达探明了主要的地层单元、基岩深度、以及洞顶崩塌的位置，也显示出了地层单元中沉积物的信息。这是一个全面探索岩棚沉积及其地球物体特征的独一无二的成果，有助于解释复杂遗址的沉积物，并未将来的调查提供有用的工具。

ABSTRACT：Ground-penetrating radar (GPR) surveys offer several advantages for non-invasively assessing stratigraphy in archaeological rockshelters, including providing information about subsurface stratigraphy and the location of features such as roof fall and bedrock. Challenges to understanding the record of human impact and site formation processes in Australian rockshelter deposits include where to position archaeological excavations, how best to determine the onset of human occupation within sequences beyond the presence of stone artefacts (which can be limited at depth owing to sampling issues) and how to resolve issues relating to stratigraphic associations. This paper demonstrates how GPR can be used to gain a better understanding of buried deposits in a Pleistocene-aged rockshelter. When compared with results from sediment magnetic susceptibility studies, GPR verified the major stratigraphic units identified at the site, the depth of bedrock and the presence of roof fall, but it also provided information on the sediment volume within the stratigraphic units. This is a unique outcome for exploring rockshelter deposits and geophysical signatures overall, aiding in the interpretation of complex site sediments and offering a useful tool for future site investigations.

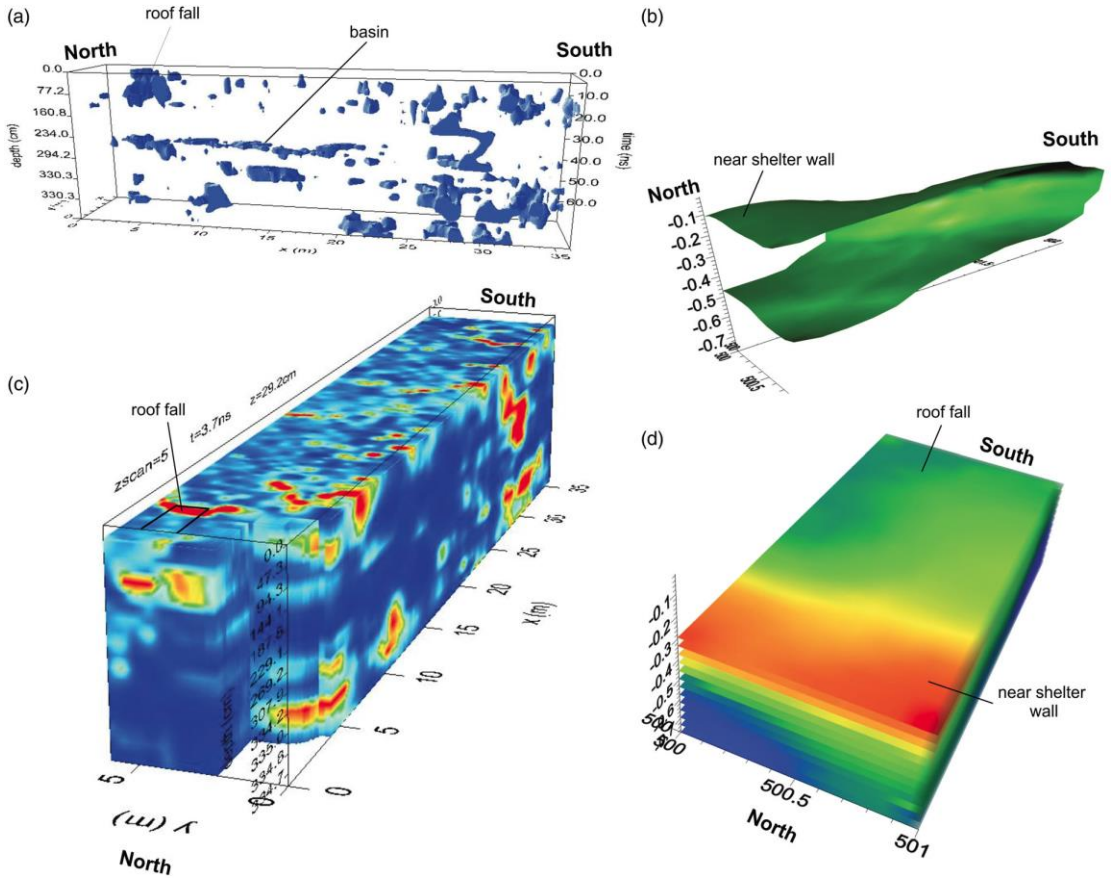

Figure 1. Isosurface rendering of the GPR data showing roof fall and the basin (a), the 3D volume cubes of the GPR (b), the isosurface rendering of the magnetic susceptibility and areas of magnetic enhancement (c), and the 3D volume magnetic susceptibility showing contrasting values for roof fall (d). Note areas in red and yellow for both datasets are strong reflections and higher susceptibility.